Atmos. Meas. Tech. Discuss., doi:10.5194/amt-2016-127, 2016
Manuscript under review for journal Atmos. Meas. Tech.
Published: 25 April 2016
© Author(s) 2016. CC-BY 3.0 License.



Atmospheric Measurement Techniques Discussions

The Zugspitze radiative closure experiment for quantifying water vapor absorption over the terrestrial and solar infrared. Part II: Accurate calibration of high spectral resolution infrared measurements of surface solar radiation

Andreas Reichert, Markus Rettinger, and Ralf Sussmann

Karlsruhe Institute of Technology, IMK-IFU, Garmisch-Partenkirchen, Germany

Correspondence to: A. Reichert (andreas.reichert2@kit.edu)

Abstract. Quantitative knowledge of water vapor absorption is crucial for accurate climate simulations. An open science question in this context concerns the strength of the water vapor continuum in the near infrared (NIR) at atmospheric temperatures, which is still to be quantified by measurements. This issue can be addressed with radiative closure experiments using solar absorption spectra. However, the spectra used for water vapor continuum quantification have to be radiometrically calibrated. We present for the first time a method that yields sufficient calibration accuracy for NIR water vapor continuum quantification in an atmospheric closure experiment. Our method combines the Langley method with spectral radiance measurements of a high-temperature blackbody calibration source (< 2000 K). The calibration scheme is demonstrated in the spectral range 2500 to 7800 cm^{-1}, but minor modifications to the method enable calibration also throughout the remainder of the NIR spectral range. The resulting uncertainty (2 σ) is below 1 % in window regions and up to 1.7 % within absorption bands. A validation of this calibration uncertainty estimate is performed by investigation of calibration self-consistency, which yields compatible results within the estimated errors for 91.1 % of the 2500 to 7800 cm^{-1}-range. A second validation effort consists in a comparison of a set of calibrated spectra to radiative transfer model calculations, which are consistent within the estimated errors for 97.7 % of the spectral range.

1 Introduction

Solar absorption spectra in the near-infrared (NIR) spectral domain contain a wealth of information on atmospheric radiative processes such as absorption of radiation by atmospheric trace gases or scattering processes by clouds and aerosols. Measurements of solar absorption spectra can also be used to obtain better quantitative knowledge of the NIR absorption properties of the most important atmospheric greenhouse gas, water vapor. In addition to numerous absorption lines attributable to vibration-rotation transitions, in the case of water vapor the so-called continuum absorption has to be taken into account. The continuum absorption has significant effects on the atmospheric radiative budget (e.g. Paynter and Ramaswamy, 2011; 2014) and, consequently, knowledge of its exact magnitude is crucial for climate models (Turner et al., 2012; Rädel et al., 2015). The magnitude of the NIR water vapor continuum has been constrained in a number of laboratory experiments (e.g. Burch, 1982; Paynter et al., 2009; Ptashnik et al., 2011). However, accurate laboratory studies cannot be performed at atmospheric temperatures, and extrapolation leads to significant errors because the temperature dependence of continuum absorption is in general not well modeled (e.g. Paynter and Ramaswamy, 2011). Setting up new experiments performed in the real atmosphere rather than in the laboratory is therefore highly desirable.

In the far- and mid-infrared spectral range (FIR and MIR), a successful way for quantification of the water vapor continuum at atmospheric temperatures has been demonstrated via so-called radiative closure experiments combining spectrally resolved atmospheric thermal emission measurements with coincident measurements of the atmospheric state (e.g. Tobin et al., 1999; Serio et al., 2008; Delamere et al., 2010). In the NIR, however, closure studies of this kind have not yet been performed, because the atmospheric thermal emission is too weak in this spectral domain. A potential solution to this problem

Atmos. Meas. Tech. Discuss., doi:10.5194/amt-2016-127, 2016
Manuscript under review for journal Atmos. Meas. Tech.
Published: 25 April 2016
© Author(s) 2016. CC-BY 3.0 License.



Atmospheric Measurement Techniques Discussions

in the NIR is the use of solar absorption spectra. We therefore aim to perform a radiative closure experiment using solar absorption spectra at the Zugspitze (47.42° N, 10.98° E, 2964 m a.s.l.) observatory. In the framework of the Network for the Detection of Atmospheric Composition Change (NDACC; Kurylo, 1991; http://www.ndacc.org/), solar FTIR measurements are regularly carried out at the Zugspitze site (Sussmann and Schäfer, 1997). However, the application of solar absorption spectra requires the observations to be radiometrically calibrated. Unfortunately, the standard solar FTIR instrumentations used within the networks NDACC or TCCON (Total Carbon Column Observing Network, http://www.tccon.caltech.edu/, Wunch et al., 2011) do not include radiometric calibration.

In the far- and mid-infrared spectral range, a calibration method for high-resolution spectral radiance measurements based on the observation of two blackbody sources at different temperatures is well established (Revercomb et al., 1988). However, there is currently no standard calibration scheme available for the NIR spectral range. Gardiner et al. (2012) proposed a calibration method based on spectral radiance measurements of a very high temperature (3000 K) blackbody source. The installation of such an extremely hot calibration source is highly challenging at remote (mountain or polar) observatories typically used for radiative closure experiments (because of the low atmospheric humidity required).

Furthermore, given the calibration accuracy of 3.3 to 5.9 % attainable with the approach proposed by Gardiner et al. (2012), significant continuum absorption could only be measured in a small fraction of the 2500 to 7800 cm^{-1} spectral range with our experimental setup. In detail, the range of integrated vertical water vapor column (IWV) covered by our data set is 1.4 to 3.3 mm. Taking into account additional sources of radiance uncertainty in our closure setup (described in detail in the companion paper Sussmann et al., same issue, hereafter referred to as Part I), and assuming the MT_CKD 2.5.2 continuum model (Mlawer et al., 2012), a calibration accuracy < 2 % is necessary to measure significant continuum absorption throughout at least 33 % of the 2500 to 7800 cm^{-1} spectral range covered by our measurements.

It is therefore the goal of this paper to demonstrate an alternative calibration scheme which overcomes these shortcomings and meets the calibration uncertainty of < 2% required for water vapor continuum quantification in the Zugspitze closure experiment. Our calibration strategy is a synergetic combination of two approaches. First, we use the Langley calibration method that allows for precise absolute calibration in selected spectral windows. Additionally, our calibration relies on spectral radiance measurements of a blackbody source (1973 K) to gain information on the shape of the calibration curve between these windows. The combined method provides sufficiently accurate radiometric calibration of NIR solar FTIR spectra to subsequently determine water vapor continuum magnitude and validate water vapor line parameters. Our approach eliminates the need for a very high temperature source only available in few designated laboratories. This paper, thereafter referred to as Part II, constitutes the second contribution to a trilogy of papers describing the Zugspitze radiative closure experiment. Part I introduces the setup of the experiment, provides a sensitivity analysis and presents results on the far-infrared water vapor continuum. Part III (Reichert et al., same issue) describes the quantification of the NIR water vapor continuum based on the radiometric calibration method provided in this study.

Our paper is organized as follows. In Sect. 2, the instrumental setup of the Zugspitze solar FTIR spectrometer, the typical configuration of the spectral radiance measurements for which the calibration is applied and the blackbody calibration source are presented. Section 3 gives a description of the combined calibration strategy, while the uncertainty associated with the calibration procedure is outlined in Sect. 4. In Sect. 5, the validation of calibration results is discussed. Finally, Sect. 6 provides a summary and conclusions.

2 Instrumental setup

2.1 Zugspitze NIR solar absorption measurements

The NIR solar absorption spectra to which the calibration is applied are measured with a solar FTIR spectrometer located at the high-altitude observatory on the summit of Mt. Zugspitze, Germany (47.42° N, 10.98° E, 2964 m a.s.l.). The spectrometer

Atmos. Meas. Tech. Discuss., doi:10.5194/amt-2016-127, 2016
Manuscript under review for journal Atmos. Meas. Tech.
Published: 25 April 2016
© Author(s) 2016. CC-BY 3.0 License.



Atmospheric Measurement Techniques Discussions

setup is described in detail in Sussmann and Schäfer (1997). Briefly, the measurements are obtained with a Bruker IFS125HR interferometer. The interferometer's field of view actively tracks the position of the center of the solar disc by means of feedback from a quadrant diode. Interferograms were recorded with a maximum optical path difference (OPD) of 45 cm and averaged over 4 to 8 scans.

Spectra are typically measured with a liquid nitrogen-cooled InSb detector (1850 to 9600 cm^{-1}) in combination with a KBr beam splitter. An alternative setup consisting of an InGaAs detector (4000 to 12800 cm^{-1}) and a CaF_2 beam splitter is available. This setup has the advantage of improved signal-to-noise ratio especially above 6000 cm^{-1} and avoids a spectral interval of low instrumental sensitivity between 5200 to 5800 cm^{-1} attributed to low transmissivity of the KBr beam splitter. However, for routine operations of the solar FTIR spectrometer, especially for the long-term determination of atmospheric trace gas column amounts and vertical profiles (e.g. Borsdorff and Sussmann, 2009; Sussmann et al., 2009; 2012; Hausmann et al., 2016), the first option is more suitable. Therefore, most spectra to be calibrated were recorded with the InSb/KBr setup, while the InGaAs/CaF_2 setup was only used in a number of single-day measurement campaigns. While the calibration scheme presented here is applicable for both configurations, we therefore focus on the InSb/KBr setup throughout the remainder of this paper.

2.2 Blackbody calibration unit

The calibration procedure makes use of a blackbody calibration source installed in the Zugspitze solar FTIR dome. The calibration source (MIKRON M330-EU, Lumasense Technologies) is shown in Fig. 1, while its technical specifications according to the manufacturer are given in Table 1. Blackbody spectra are measured with the solar FTIR using the solar tracker optics and an additional gold-coated 90° off-axis mirror. The thermal radiation emitted by the calibration source is directed to the solar tracker by means of the additional off-axis mirror, whose distance to the blackbody cavity interior is set to its focal length of f = 478 mm. Blackbody source and off-axis mirror are aligned in order to produce a parallel beam with a diameter of 156 mm that incides at a 90° angle on the solar tracker elevation mirror.

3 Calibration method

Our approach comprises a Langley-type calibration described in Sect. 3.1 and a blackbody calibration presented in Sect. 3.2. Our new calibration strategy is a combination of both as explained in Sect. 3.3.

3.1. Langley calibration

3.1.1 General description

The Langley method (e.g. Liou, 2002) has been frequently used for solar constant determination or calibration of sun photometers. It relies on repeated measurements of solar irradiance or radiance at a range of solar zenith angles. According to the Beer-Bouguer-Lambert law, the direct solar irradiance at a wavenumber v observed at the surface is given by

$$\boldsymbol{F}(v) = \boldsymbol{F}_0(v) \cdot \exp(-\boldsymbol{k}(v) \cdot m) \,, \quad (1)$$

where $\boldsymbol{F}_0(v)$ denotes the extra-atmospheric solar irradiance, $\boldsymbol{k}(v)$ the atmospheric absorption coefficient and m the relative air mass, i.e. the ratio of the air mass along the line of sight of the observer to the sun and the air mass in zenith direction. Taking the logarithm of Eq. (1) results in the linear relation

$$\ln(\boldsymbol{F}(v)) = \ln(\boldsymbol{F}_0(v)) - \boldsymbol{k}(v) \cdot m \,. \quad (2)$$

Equation (2) implies that the logarithm of the extra-atmospheric solar irradiance can be calculated by measuring solar irradiance at a range of air mass values and interpolation of the results to air mass 0 according to the best fit linear relation between air mass and logarithm of measured irradiance. The resulting value of $\boldsymbol{F}_0(v)$ can then be compared to the known extra-atmospheric solar spectrum (ESS) to yield a radiometric calibration at that wavenumber. An inversion of this scheme,

Atmos. Meas. Tech. Discuss., doi:10.5194/amt-2016-127, 2016
Manuscript under review for journal Atmos. Meas. Tech.
Published: 25 April 2016
© Author(s) 2016. CC-BY 3.0 License.



Atmospheric Measurement Techniques Discussions

i.e. deducing an ESS from calibrated solar FTIR measurements was presented by Menang et al. (2013).

Equation (2) is only fulfilled if atmospheric properties like IWV or aerosol optical thickness do not vary during the measurements. Since IWV varies significantly even over short time scales (e.g. Kämpfer et al., 2013; Vogelmann et al., 2015), accurate Langley measurements in spectral regions with significant absorption by water vapor have to be carried out within short time intervals, i.e. at high solar zenith angles. Refraction has a significant influence at high solar zenith angles. In order to include refraction effects, air mass values used in this study were computed by means of ray tracing calculations. Since atmospheric absorption is dominated by water vapor for most spectral points considered in this study, instead of using the air column, the related water vapor column was utilized as an air mass input to the Langley fits.

3.1.2 Selection of suitable spectra

Langley calibration coefficients were determined from daily sets of selected solar FTIR spectra recorded under apparently cloud-free conditions at 0.02 cm^{-1} resolution (where resolution is defined as 0.9/OPD) and averaged over 4 scans. Several effects may lead to radiance measurements inconsistent with Eq. (2) and thereby lead to biased calibration results. A first issue is related to the fact that the instrument's field of view (FOV) covers different areas of the solar tracker mirrors throughout the day. This is a result of inaccuracies in mirror alignment. Mirror aging and dirtying leads to spatially inhomogeneous reflectivity of the tracker mirrors. Therefore, even if the atmospheric radiance is constant, a spurious variation in measured radiance depending on the instrument's viewing direction can be detected, which leads to calibration errors. Thin clouds in the line of sight of the solar FTIR reduce the measured radiance and therefore also bias the calibration result.

We use a preliminary Langley plot to select the spectra which are least affected by cloud, IWV variation, and FOV effects:

i) A spectral interval with little molecular absorption, namely 4300 $cm^{-1} < \nu < 4350\,cm^{-1}$, was selected. Within this interval, Langley plots according to Eq. (2) were generated using the mean radiance for spectral points with the lowest atmospheric optical depth (red and green points in Fig. 2).

ii) A first estimate of the linear relation avoiding cloud and FOV bias (continuous black line in Fig. 2) was fitted using the spectra with the highest mean radiance within each air mass bin (width $\Delta m = 1$). Air mass bins for which the mean radiance did not decrease with increasing air mass as expected for cloud-free measurements were discarded.

iii) The maximum deviation from the ideal linear relation not attributable to FOV influence or IWV temporal variability was calculated. The FOV effect was estimated as outlined in Sect. 4.1. Based on the results of Vogelmann et al. (2015), the expected IWV variability was estimated to be about 1 mm during typical Langley measurements with 1-2 h duration.

iv) Spectra consistent with the linear relation determined in ii) minus the maximum deviation estimated in iii) measured at an air mass less than 9.0 were selected for further analysis (dashed line in Fig. 2). An air mass threshold is required since, at very high solar zenith angles, air mass calculation becomes increasingly inaccurate, and air mass changes significantly during the spectral averaging period. The selected spectra are shown as green circles in Fig. 2, while discarded spectra are shown in red.

We further processed Langley datasets with a sufficiently high number of selected spectra according to the selection criteria presented above (> 10 measurements) over an air mass range of at least $\Delta m = 2$ and with IWV < 5 mm, since moist atmospheric conditions reduce the fraction of spectral intervals suitable for accurate calibration. Langley measurements fulfilling these criteria were recorded on 12 Dec. 2013 and 13 Dec. 2013.

3.1.3 Langley fit and spectral window selection

A number of issues have to be considered before generating Langley fits according to Eq. (2) using the selected spectra. During measurements, the line of sight of the solar FTIR continuously tracks the position of the center of the solar disc. Sun tracking inaccuracies influence the Langley measurements due to the spatial inhomogeneity of the solar emission, the

Atmos. Meas. Tech. Discuss., doi:10.5194/amt-2016-127, 2016
Manuscript under review for journal Atmos. Meas. Tech.
Published: 25 April 2016
© Author(s) 2016. CC-BY 3.0 License.



so-called solar limb darkening. Furthermore, mispointing leads to erroneous air mass input for the Langley fit. As outlined in Reichert et al. (2015), systematic mispointing can be determined using multiple measurements of solar line Doppler shifts at different orientations of the solar rotation axis. Using this method, mispointing-corrected air mass values can be calculated as an input to the Langley fits. The effect of solar limb darkening can be corrected for using the analytical description of relative intensity of NIR solar radiation depending on the fractional radius r given by Hestroffer and Magnan (1998),

$$I(r) = (1 - r^2)^{\alpha/2}\,, \tag{3}$$

where $\alpha = -0.023 + 0.292 \cdot 10^{-4}\,\mathrm{cm} \cdot \nu$. The mispointing correction consists in multiplying the calibration result by $I(r)$, where r designates the norm of the mispointing divided by the apparent solar radius.

The Langley calibration method requires knowledge of the ESS. In this study, we use the semi-empirical synthetic ESS of Kurucz (2005). This extra-atmospheric spectrum is widely adopted for atmospheric radiative transfer calculations due to its high spectral resolution (radiance spectra are provided with 0.1 cm^{-1} point spacing) and its wide spectral range (0 to 50000 cm^{-1}). Furthermore, we use the ESS proposed by Thuillier et al. (2003) that is based on satellite observations. This spectrum covers a range of 0.1 to 2400 nm with a NIR spectral resolution of 0.5 nm. This resolution allows for the identification of broad solar lines but does not provide fine enough resolution for a detailed representation of solar line shapes. An advantage of the Thuillier et al. (2003) solar spectrum over the Kurucz (2005) spectrum is that it includes an uncertainty estimate that can be used in the uncertainty analysis of the radiometric calibration provided in Sect. 4.1.

The uncertainty of the Langley calibration varies strongly throughout the spectrum. Therefore, it is necessary to select spectral windows in which accurate Langley results can be obtained. Figure 3 shows the selection steps applied to the Langley results. In the following, several selection criteria make use of upper or lower linear envelopes to the spectra. These envelopes are constructed by selecting the highest or lowest values in the spectra within each wavenumber bin of a given width. The envelope is then constructed by linear interpolation between these selected points. In detail, the following selection criteria were used:

i) Spectral points within solar lines are excluded due to the higher ESS radiance uncertainty in these regions. In detail, all points with ESS radiance more than 1 % below the upper linear envelope using 20 cm^{-1} width bins are excluded (grey points in Fig. 3).

ii) All spectral points for which the relative Langley fit uncertainty was above 0.4 % were discarded (orange points in Fig. 3).

iii) Furthermore, regions within solar lines not included in the ESS of Kurucz (2005) and points with spurious low fit uncertainty due to radiance measurement noise were excluded. For this purpose, all points for which the standard deviation of Langley calibration results within a 0.1 cm^{-1} – wide interval around any given spectral point exceeds 0.3 % were excluded (purple points in Fig. 3).

Blackbody spectral radiance measurements (see Sect. 3.2) show that the solar FTIR calibration curve varies only slowly with wavenumber. The filtered Langley results (blue points in Fig. 3) were therefore averaged (error-weighted mean using Langley fit uncertainties) over 20 cm^{-1}-windows in order to further reduce statistical uncertainty. The final averaged Langley calibration coefficients are shown as red circles in Fig. 3 and are designated “Langley points” throughout the remainder of this study.

3.2. Blackbody calibration

Spectral radiance measurements of the blackbody calibration source described in Sect. 2.2 are used to determine the shape of the calibration curve in spectral intervals between the points suitable for precise Langley calibration. Contrary to the calibration approach described by Gardiner et al. (2012), using a source with of 3000 K, a lower cavity temperature of 1973.15 K can be used in the Zugspitze experiment due to the combination with Langley measurements. Blackbody calibration spectra were measured with a resolution of 0.02 cm^{-1}.

Atmos. Meas. Tech. Discuss., doi:10.5194/amt-2016-127, 2016
Manuscript under review for journal Atmos. Meas. Tech.
Published: 25 April 2016
© Author(s) 2016. CC-BY 3.0 License.



Atmospheric Measurement Techniques Discussions

In order to avoid biased calibration results due to water vapor line absorption in the blackbody spectra, only measurements with an atmospheric water vapor density $\rho_{H2O} < 1\,g/m^3$ at the Zugspitze summit observatory were considered for calibration. Spectra are averaged over time intervals with stable blackbody radiance, i.e. periods for which changes in air temperature inside the solar FTIR dome could be compensated by the blackbody thermostat.

Only spectral points outside water vapor lines were considered to avoid bias in the calibration. In detail, only points less than $10\,\sigma$ (where σ designates the mean measurement noise) below the upper envelope of the measured spectra were selected (black spectrum in Fig. 4). The influence of measurement noise can then be further reduced by applying a median filter ($20\,cm^{-1}$ width) to the spectra (red spectrum in Fig. 4). Finally, the blackbody calibration curve $\boldsymbol{c}_{bb}(\nu)$ is calculated from the averaged spectra by dividing the Planck curve at the cavity temperature T_{bb} by the measured spectrum.

3.3. Combined calibration

The combined calibration strategy takes advantage of the low-uncertainty Langley calibration at suitable spectral points (see Sect. 3.1). In between the Langley points, the shape of the calibration curve is constrained by the blackbody measurements (see Sect. 3.2). The combined calibration curve $\boldsymbol{c}(\nu)$ is given by the relation

$$\boldsymbol{c}(\nu) = \boldsymbol{c}_{bb}(\nu) \cdot \boldsymbol{c}_{lan,linear}(\nu) / \boldsymbol{c}_{bb,linear}(\nu)\,, \quad (4)$$

where $\boldsymbol{c}_{bb}$ designates the blackbody calibration curve derived according to Sect. 3.2. $\boldsymbol{c}_{lan,linear}$ and $\boldsymbol{c}_{bb,linear}$ designate linear interpolations constructed as follows: at the Langley calibration points, $\boldsymbol{c}_{lan,linear}$ and $\boldsymbol{c}_{bb,linear}$ are set to the Langley and blackbody calibration results, respectively. In between these points, $\boldsymbol{c}_{lan,linear}$ and $\boldsymbol{c}_{bb,linear}$ are calculated by linear interpolation. The combined calibration curve calculated according to Eq. (4) from blackbody measurements made on 24 Feb. 2014 and Langley measurements made on 13 Dec. 2013 is shown in Fig. 5.

4 Calibration uncertainty

4.1 Contributions from Langley calibration

Several contributions to the calibration uncertainty budget are associated with the Langley measurements. A first contribution results from the uncertainty of the Langley fit. This contribution is calculated as an error-weighted mean over the 2-σ fit uncertainties of the spectral points contributing to each Langley point. In between Langley points, the uncertainty estimate is obtained by linear interpolation. The Langley contribution to the calibration uncertainty ranges from 0.35 to 0.72 % throughout the spectral range considered for calibration and is shown in Fig. 6 (blue line).

Furthermore, a combination of spatially inhomogeneous reflectivity of the solar tracker mirrors and the fact that the area covered by the instrument's FOV on the mirrors changes over time leads to spurious radiance variations in the Langley calibration. To obtain an estimate of this error, the time-dependent position of the instrument FOV on the tracker elevation mirror was measured using an outgoing laser beam aligned with the instrument's optical axis. In the spectral regions with least atmospheric absorption, the diurnal variation of the measured signal is about 5 %. A conservative estimate of the FOV-related error is obtained assuming that this diurnal variation is solely due to mirror inhomogeneity and that mirror reflectivity drops abruptly by this amount outside the area initially covered by the FOV. Consequently, the error estimate is obtained by multiplying the 5 % reflectivity change with the fraction by which the area within the field of view has changed throughout the calibration time interval. The resulting Langley calibration uncertainty due to mirror inhomogeneity is ~0.2 % (cyan line in Fig. 6).

The accuracy of the Langley results is also limited by errors in the air mass values used for the fit. Firstly, this is due inaccurate solar zenith angle input. A second and by far dominant effect is due to the fact that the relative air mass for absorbing species with different concentration profiles is not equal for a given solar zenith angle. Depending on the spectral region, the dominant contribution to atmospheric OD for most Langley points is either due to water vapor or aerosols. For our

Atmos. Meas. Tech. Discuss., doi:10.5194/amt-2016-127, 2016
Manuscript under review for journal Atmos. Meas. Tech.
Published: 25 April 2016
© Author(s) 2016. CC-BY 3.0 License.



Atmospheric Measurement Techniques Discussions

analysis, water vapor relative air masses were used. The difference of the calibration results when performing the analysis with relative air columns instead of water vapor columns is up to 0.5 % and was taken as an estimate of the air mass related calibration uncertainty (see orange line in Fig. 6).

An additional uncertainty contribution of up to 0.25 % results from the uncertainty of the mispointing correction outlined in Sect. 3.1.3 (purple line in Fig. 6). This contribution includes two effects related to the mispointing uncertainty: the effects of air mass uncertainty in the Langley fit and the uncertainty in the solar limb darkening correction outlined in Sect. 3.1.3. A further uncertainty contribution is associated with the ESS used in the Langley calibration. The 2-σ uncertainty of the Thuillier et al. (2003) spectrum is reported to be in the range of 1.2 % at 4000 cm^{-1} to 1.8 % at 8000 cm^{-1}, as shown in Fig. 6 (yellow lines). No uncertainty estimate was provided by the authors for the spectrum of Kurucz (2005).

4.2 Blackbody calibration uncertainty

A further contribution to the calibration uncertainty results from the blackbody measurements. The blackbody calibration curve uncertainty was calculated as two times the standard deviation of all normalized blackbody calibration curves recorded under suitably dry atmospheric conditions (near-surface atmospheric water vapor density $\rho_{H2O} < 1$ g/m^3). These measurements include spectra at T_{bb} = 1923.15 K to 1973.15 K cavity temperature. The relative error in the combined calibration curve resulting from the uncertainty of the blackbody measurements does not exceed 1.5 % and is shown in Fig. 6 (red lines).

4.3 Combined calibration uncertainty estimate

The combined calibration according to Eq. (4) is based on the assumption that the blackbody calibration curve between suitable Langley points can be approximately described by multiplying the Langley calibration curve with a linear function, i.e. that the following relation is fulfilled:

$$\boldsymbol{c}_{bb}(\nu)/\boldsymbol{c}_{bb,linear}(\nu) \approx \boldsymbol{c}_{lan}(\nu)/\boldsymbol{c}_{lan,linear}(\nu) \quad (5)$$

Equation (5) is not exactly fulfilled e.g. if the reflectivity of the additional off-axis mirror used for blackbody measurements does not vary linearly between Langley points. As a consequence, an additional contribution to the calibration uncertainty results from the use of the combined approach presented in Sect. 3.3. In order to obtain an estimate of this shape error contribution, the following procedure was applied:

i) The calibration error induced by omitting the Langley result at each single Langley spectral point ν_i and using only the neighboring points ν_{i-1} and ν_{i+1} is calculated. A preliminary shape error curve is then constructed from the error values at all ν_i by linear interpolation.

ii) The final shape error estimate is set to 0 at all Langley points ν_i according to Eq. (4). At all spectral points halfway between Langley points, i.e. at $(\nu_{i+1} - \nu_i) / 2$, the final error estimate is set to the value of the preliminary curve determined in i).

iii) At spectral points between those mentioned in ii), the estimated error is calculated by linear interpolation.

The shape error generally increases with increasing Langley point spacing. By construction, the error estimate resulting from the method given above corresponds to a mean Langley point spacing two times as large as the real spacing. The error estimate provided above is therefore expected to overestimate the real errors in most cases. The final shape error estimate is shown as a green curve in Fig. 6 and is up to 0.5 % throughout the spectral range considered.

Thermal emission from instrument parts at room temperature contributes a fraction of less than 10^{-5} to the measured solar radiance within the considered spectral interval. Contrary to the situation for instruments operating in the far-infrared spectral range, this contribution is therefore of negligible importance for the calibration error budget. Within the Zugspitze radiative closure experiment, the same ESS is used for Langley calibration and radiative transfer calculations. Therefore, the accuracy of the water vapor continuum optical depth derived in closure experiments from the calibrated spectra is not heavily affected

Atmos. Meas. Tech. Discuss., doi:10.5194/amt-2016-127, 2016
Manuscript under review for journal Atmos. Meas. Tech.
Published: 25 April 2016
© Author(s) 2016. CC-BY 3.0 License.



by errors in the extra-atmospheric solar spectrum. The overall uncertainty relevant for water vapor continuum detection, i.e. not including the extra-atmospheric solar spectrum contribution, is shown in Fig. 6 (black lines). It is typically below 1 % within the calibration range, except for regions with sparse Langley point density or low beam splitter transmissivity where maxima of up to 1.7 % uncertainty exist. The error budget including the solar spectrum (grey lines in Fig. 6) is about 1.5 - 2 % throughout the 4000 to 7800 cm^{-1} wavenumber range.

5 Validation of results

5.1 Self consistency

A first method to validate the calibration results and the associated error estimate is to investigate the self-consistency of different calibration cases, i.e. the reproducibility of the calibration. The self-consistency of blackbody measurements is presented in Sect. 4.2. This result is then used as an estimate of the blackbody-related contribution to the total calibration uncertainty. As outlined in Sect. 4.2, this uncertainty contribution does not exceed 1.5 % throughout the spectral interval considered for calibration. The reproducibility of the Langley results is estimated by comparing the Langley measurements made on 12 Dec. 2013 with the ones made on 13 Dec. 2013. As shown in the Fig. 7a, the calibration curves determined from those two Langley measurements typically differ by less than 1 % outside absorption bands. In regions with sparse coverage of Langley points, i.e. within water vapor absorption bands, differences are typically around 1.5 %. Throughout 91.1 % of the calibration spectral range (2500 to 7800 cm^{-1}), the calibration curves are consistent within the calibration uncertainty estimate of Sect. 4 (grey shaded area in Fig. 7a). This extensive consistency consolidates the validity of the error budget presented in Sect. 4.

5.2. Comparison to model results

The validity of the calibration error estimate provided in Sect. 4 can be further investigated by a closure of calibrated spectra with synthetic solar absorption spectra obtained by radiative transfer model calculations. This analysis enables to detect any large deviations of the real calibration accuracy from the uncertainty estimate given in Sect. 4. Note, however, that in addition to the calibration uncertainty further sources of radiance uncertainty contribute in the closure setup, e.g. IWV uncertainty or uncertainties related to the water vapor continuum. Therefore, minor deviations from the 1 to 1.7 %-uncertainty estimate may remain undetected in the comparison analysis.

In detail, a set of calibrated spectra is compared to synthetic spectra obtained with the LBLRTM radiative transfer model (Clough et al., 2005). The atmospheric state used as an input to the LBLRTM calculations was determined as outlined in Part I. In summary, we use water vapor column data retrieved from the solar FTIR spectra. Water vapor profiles were set according to four times-daily National Center for Environmental Prediction (NCEP) resimulation data, while for temperature profiles we used a combination of NCEP reanalysis results and a fitted near-surface profile obtained from FIR thermal emission spectra. CO_2, CH_4, and N_2O column values were measured with the nearby Garmisch solar FTIR. Aerosol optical depth was constrained with sun photometer measurements.

For the validation analysis, we used spectra measured under clear sky conditions during the Dec. 2013 to Feb. 2014 period during which no realignment or other modifications to the spectrometer were performed. All spectra with an air mass greater than 9.0, i.e. a solar zenith angle greater than ~84° where discarded due to increasing inaccuracies in the ray tracing calculation and significant air mass variation during the spectral averaging period at high zenith angles. Additionally, the validation dataset only includes spectra for which the radiance uncertainty due to FOV variations on the tracker mirrors (see Sect. 4.1) is negligible (< 0.1 %). These selection thresholds lead to a validation dataset of 52 spectra. For calibration, the 13 Dec. 2013 Langley and 24 Feb. 2014 blackbody results were used.

Atmos. Meas. Tech. Discuss., doi:10.5194/amt-2016-127, 2016
Manuscript under review for journal Atmos. Meas. Tech.
Published: 25 April 2016
© Author(s) 2016. CC-BY 3.0 License.



Atmospheric Measurement Techniques Discussions

The corresponding synthetic spectra were then computed for all calibrated spectra in the validation dataset. Figure 7b shows the mean measured (black) and synthetic (red) radiance for this set of spectra. The mean spectral residuals, i.e. the difference between synthetic and measured radiance is shown in red in Fig.7c, while the standard deviation of the residuals is shown in grey. Quantitatively accurate closure is only possible outside solar lines due the high ESS uncertainty within the lines. We therefore exclude these regions from the comparison based on the selection criterion provided in Sect. 3.1.3. Within atmospheric lines, the uncertainty of the closure is dominated by atmospheric state and line parameter uncertainties and therefore does not provide substantial insights on the calibration accuracy. We therefore discarded these spectral points by excluding al spectral below 99 % of the upper envelope to the mean radiance in 20 cm^{-1}-wide bins. As outlined in Sect. 3.2, the blackbody measurements demonstrate that the calibration curve varies only slowly with wavenumber and contains no narrow line-like features. Therefore, it is sufficient to validate the calibration results in suitable windows between spectral lines as outlined above. The residuals shown in Fig. 7 and their further quantitative analysis given hereafter refer to these suitable validation windows.

The accuracy of the calibration uncertainty provided in Sect. 4 can be assessed by comparing the mean spectral residuals to their estimated uncertainty (blue lines in Fig. 7c). In addition to the calibration uncertainty according to Sect. 4, the residual uncertainty given in Fig. 7 contains several further contributions. These contributions describe the atmospheric state uncertainty and further contributions related to the solar FTIR spectral radiance measurements. A detailed assessment of this closure uncertainty budget is given in Part I, Sect. 6. In addition to the contributions listed in Part I, the uncertainty contribution associated with the water continuum absorption has to be taken into account. Since no uncertainty is provided for the MT_CKD 2.5.2-model (Mlawer et al., 2012) used in the synthetic spectra calculation, the continuum error estimate was set to the difference between the upper and lower end of continuum results provided by recent studies, namely the studies by Ptashnik et al. (2012; 2013) and the MT_CKD 2.5.2-model. A more detailed description of these data sets is given in Part III. Note that since for both Langley calibration and model calculations the same extra-atmospheric solar spectrum is used, the closure validation does not provide information on the accuracy of the used ESS.

As visible in Fig. 7c, the mean residuals show very good consistency with the estimated uncertainty. In detail, a fraction of 97.7 % of the residual values lies within the 2-σ residual uncertainty estimate. The mean residuals correspond to 1.2 % of the measured radiance at each spectral point on average for the suitable comparison windows. This extensive agreement of the mean residuals with the uncertainty estimate further indicates the validity of the calibration uncertainty budget presented in Sect. 4.

6 Summary and conclusions

We presented a novel radiometric calibration strategy for high resolution solar FTIR spectral radiance measurements in the NIR and MIR which relies on a combination of the Langley method with radiance measurements of a blackbody source. While the Langley method yields highly accurate calibration results at a number of suitable spectral points, the blackbody measurements constrain the shape of the calibration curve in between these points. The combined calibration scheme therefore provides a 2-σ calibration uncertainty of about 1.0-1.7 % throughout the spectral range employed for calibration (2500 to 7800 cm^{-1}), which constitutes a significant improvement compared to the uncertainty of 3.3−5.9 % reached in previous studies. Furthermore, as opposed to the previously available scheme by Gardiner et al. (2012), the combined calibration scheme does not require access to a very high temperature (3000 K) blackbody source and can therefore be implemented at a higher number of sites including the Zugspitze summit observatory.

The calibration scheme was implemented in the spectral range 2500 to 7800 cm^{-1}. At lower wavenumber values, thermal emission from the instrument itself becomes non-negligible. Therefore, alternative methods such as the widely used method introduced by Revercomb et al. (1988) are more suitable for calibration in this spectral range. The proposed new method can, however, be implemented with minor changes in the spectral range beyond 7800 cm^{-1}. Substitution of the solar FTIR detector

Atmos. Meas. Tech. Discuss., doi:10.5194/amt-2016-127, 2016
Manuscript under review for journal Atmos. Meas. Tech.
Published: 25 April 2016
© Author(s) 2016. CC-BY 3.0 License.



Atmospheric Measurement Techniques Discussions

and beam splitter (InGaAs detector and CaF_2 beam splitter instead of InSb/KBr) allows for an extension of the calibration range up to about 9000 cm^{-1}, while the use of a higher temperature blackbody source or standard lamp enables calibration at even higher wavenumber values until the visible spectral range.

An assessment of the calibration uncertainty budget was made, containing contributions from the Langley fit, the blackbody measurements, the combination of both techniques in a single calibration curve, the solar tracker pointing accuracy and the accuracy of the extra-atmospheric solar spectrum. The estimated uncertainty is below 1 % in window regions and up to 1.7 % within absorption bands. The calibration results were validated by investigation of self-consistency for different calibration measurements and radiative closure with line-by-line model calculations. Both validation efforts confirm the 1.0–1.7 % uncertainty estimate.

The presented scheme therefore fulfills the main goal, i.e. to provide sufficiently accurate radiometric calibration of solar FTIR spectra for the use in radiative closure experiments. Most notably, the calibration scheme thereby enables for the first time a quantification of the water vapor continuum in the NIR spectral range under atmospheric conditions, and the corresponding results are presented in the companion publication Part III.

Acknowledgements. We thank H. P. Schmid (KIT/IMK-IFU) for his continual interest in this work. Funding by the Bavarian State Ministry of the Environment and Consumer Protection (contracts TLK01U-49581 and VAO-II TP I/01) and Deutsche Bundesstiftung Umwelt is gratefully acknowledged. We furthermore thank U. Köhler (Meteorologisches Observatorium Hohenpeissenberg, DWD) for providing ozone column measurements, M. Wiegner (LMU München) for access to sun photometer measurement data, P. Hausmann (KIT/IMK-IFU) for providing IWV retrievals, and F. Hase (KIT/IMK-ASF) for valuable discussions. We thank for support by the Deutsche Forschungsgemeinschaft and Open Access Publishing Fund of the Karlsruhe Institute of Technology.

Atmos. Meas. Tech. Discuss., doi:10.5194/amt-2016-127, 2016
Manuscript under review for journal Atmos. Meas. Tech.
Published: 25 April 2016
© Author(s) 2016. CC-BY 3.0 License.



Atmospheric Measurement Techniques Discussions

References

Burch, D. E.: Continuum absorption by H_2O. Report AFGL-TR-81-0300, Air Force Geophys. Laboratory, Hanscom AFB, MA, 1982.

Borsdorff, T. and Sussmann, R.: On seasonality of stratomesospheric CO above midlatitudes: New insight from solar FTIR spectrometry at Zugspitze and Garmisch, Geophys. Res. Lett., 36, L21804, doi:10.1029/2009GL040056, 2009.

Delamere, J. S., Clough, S. A., Payne, V. H., Mlawer, E. J. Turner, D. D., and Gamache, R. R.: A far-infrared radiative closure study in the Arctic: Application to water vapor, J. Geophys. Res., 115, D17106, doi:10.1029/2009JD012968, 2010.

Clough, S. A., Shephard, M. W., Mlawer, E. J., Delamere, J. S., Iacono, M. J., Cady-Pereira, K., Boukabara, S., and Brown P. D.: Atmospheric radiative transfer modeling: a summary of the AER codes, Short Communication, J. Quant. Spectrosc. Radiat. Transfer, 91, 233-244, doi:10.1016/j.jqsrt.2004.05.058, 2005.

Gardiner, T. D., Coleman, M., Browning, H., Tallis, L., Ptashnik, I. V., and Shine, K. P.: Absolute high spectral resolution measurements of surface solar radiation for detection of water vapour continuum absorption, Phil. Trans. R. Soc. A, 370, 2590–2610, doi:10.1098/rsta.2011.0221, 2012.

Hestroffer, D., and Magnan, C.: Wavelength dependency of the Solar limb darkening, Astron. Astrophys. 333, 338–342, 1998.

Kämpfer, N.: Monitoring atmospheric water vapour, Ground-Based Remote Sensing and In-situ Methods, ISSI Scientific Report Series, Vol. 10, Springer, New York, doi:10.1007/978-1-4614-3909-7, 2013.

Kurucz, R. L.: The Solar Irradiance by Computation (obtained online from http://kurucz.harvard.edu/sun.html), 2005.

Kurylo, M. J.: Network for the detection of stratospheric change, Proc. SPIE 1491, P. Soc. Photo-Opt. Ins., 168 (September 1, 1991), doi:10.1117/12.46658, 1991.

Liou, K. N.: An Introduction to Atmospheric Radiation, Academic Press, Oxford, England, 583 pp., doi:10.1256/003590003102695746, 2002.

Menang, K. P., Coleman, M. D., Gardiner, T. D., Ptashnik, I. V., and Shine, K. P.: A high-resolution near-infrared extraterrestrial solar spectrum derived from ground-based Fourier transform spectrometer measurements, J. Geophys. Res. Atmos., 118, 5319–5331, doi:10.1002/jgrd.50425, 2013.

Mlawer, E. J., Payne, V. H., Moncet, J., Delamere, J. S., Alvarado, M. J., and Tobin, D.C.: Development and recent evaluation of the MT_CKD model of continuum absorption, Phil. Trans. R. Soc. A, 370, 1-37, doi:10.1098:rsta.2011.0295, 2012.

Paynter, D. J., Ptashnik, I. V., Shine, K. P., Smith, K. M., McPheat, R.A., and Williams, R. G.: Laboratory measurements of the water vapor continuum in the 1200–8000 cm_1 region between 293 K and 351 K, J. Geophys. Res., 114, D21301, doi:10.1029/2008JD011355, 2009.

Paynter, D. J. and Ramaswamy, V.: An assessment of recent water vapor continuum measurements upon longwave and shortwave radiative transfer, J. Geophys. Res., 116, 2156-2202, doi:10.1029/2010JD015505, 2011.

Paynter, D. J. and Ramaswamy, V.: Investigating the impact of the shortwave water vapor continuum upon climate simulations using GFDL global models, J. Geophys. Res. Atmos., 119, 10,720–10,737, doi:10.1002/2014JD021881, 2014.

Ptashnik, I. V., McPheat, R. A., Shine, K. P., Smith, K. M., and Williams, R. G.: Water vapor self-continuum absorption in near-infrared windows derived from laboratory measurements, J. Geophys. Res., 116, D16305, doi:10.1029/2011JD015603, 2011.

Ptashnik, I. V., McPheat, R. A., Shine, K. P., Smith, K. M., and Williams, R. G.: Water vapour foreign-continuum absorption in near-infrared windows from laboratory measurements, Phil. Trans. R. Soc. A, 370, 2557-2577, doi:10.1098/rsta.2011.0218, 2012.

Ptashnik, I. V., Petrova, T. M., Ponomarev, Yu. N., Shine, K. P., Solodov, A. A., and Solodov, A. M.: Near-infrared water vapour self-continuum at close to room temperature. J. Quant. Spectrosc. Radiat. Transf, 120, 23-35,

© Author(s) 2016. CC-BY 3.0 License.



doi:10.1016/j.jqsrt.2013.02.016, 2013.

Rädel, G., Shine, K. P., and Ptashnik, I. V.: Global radiative and climate effect of the water vapour continuum at visible and near-infrared wavelengths, Q. J. R. Meteorol. Soc., 141, 727–738, doi:10.1002/qj.2385, 2015.

Reichert, A., Hausmann, P., and Sussmann, R.: Pointing errors in solar absorption spectrometry – correction scheme and its validation, Atmos. Meas. Tech., 8, 3715-3728, doi:10.5194/amt-8-3715-2015, 2015.

Revercomb, H. E., Buijs, H., Howell, H. B, LaPorte, D. D., Smith, W. L., and Sromovsk, L. A.: Radiometric calibration of IR Fourier transform spectrometers: solution to a problem with the High-Resolution Interferometer Sounder, Appl. Opt., 27, 3210-3218, doi:10.1364/AO.27.003210, 1988.

Serio, C., Masiello, G., Esposito, F., Di Girolamo, P., Di Iorio, T., Palchetti, L., Bianchini, G., Muscari, G., Pavese, G., Rizzi, R., Carli, B., and Cuomo, V.: Retrieval of foreign-broadened water vapor continuum coefficients from emitted spectral radiance in the H_2O rotational band from 240 to 590 cm^{-1}, Opt Express., 16(20), 15816-33, doi:10.1364/OE.16.015816, 2008.

Sussmann, R., and Schäfer, K.: Infrared spectroscopy of tropospheric trace gases: combined analysis of horizontal and vertical column abundances, Appl. Opt., 36, 735-741, doi:10.1364/AO.36.000735, 1997.

Sussmann, R., Borsdorff, T., Rettinger, M., Camy-Peyret, C., Demoulin, P., Duchatelet, P., Mahieu, E., and Servais, C.: Harmonized retrieval of column-integrated atmospheric water vapor from the FTIR network – first examples for long-term records and station trends, Atmos. Chem. Phys., 9, 8987-8999, doi:10.5194/acp-9-8987-2009, 2009.

Sussmann, R., Forster, F., Rettinger, M., and Bousquet, P.: Renewed methane increase for five years (2007-2011) observed by solar FTIR spectrometry, Atmos. Chem. Phys., 12, 4885-4891, doi:10.5194/acp-12-4885-2012, 2012.

Hausmann, P., Sussmann, R., and Smale, D.: Contribution of oil and natural gas production to renewed increase in atmospheric methane (2007–2014): top–down estimate from ethane and methane column observations, Atmos. Chem. Phys., 16, 3227-3244, doi:10.5194/acp-16-3227-2016, 2016.

Thuillier, G., Hersé, M., Labs, D., Peetermans, W., Gillotay, D., Simon, P., and Mandel, H.: The solar spectral irradiance from 200 to 2400 nm as measured by the SOLSPEC spectrometer from the ATLAS and EURECA missions, Sol. Phys., 214, 1–22, doi:10.1023/A:1024048429145, 2003.

Tobin, D. C., Best, F. A., Brown, P. D., Clough, S. A., Dedecker, R. G., Ellingson, R. G., Garcia, R. K., Howell, H.B., Knuteson, R. O., Mlawer, E. J., Revercomb, H. E., Short, J. F., van Delst, P. F., and Walden, V. P.: Downwelling spectral radiance observations at the SHEBA ice station: Water vapor continuum measurements from 17-26 μm, J. Geophys. Res., 104, 2081-2092, doi:10.1029/1998JD200057, 1999.

Turner, D. D., Merrelli, A., Vimont, D., and Mlawer, E. J.: Impact of modifying the longwave water vapor continuum absorption model on community Earth system model simulations, J. Geophys. Res., 117, D04106, doi:10.1029/2011JD016440, 2012.

Vogelmann, H., Sussmann, R., Trickl, T., and Reichert, A.: Spatio-temporal variability of water vapor investigated by lidar and FTIR vertical soundings above Mt. Zugspitze, Atmos. Chem. Phys., 15, 3135–3148, doi:10.5194/acp-15-3135-2015, 2015.

Wunch, D., Toon, G. C., Blavier, J.-F. L., Washenfelder, R. A., Notholt, J., Connor, B. J., Griffith, D. W. T., Sherlock, V., and Wennberg, P. O.: The total carbon column observing network, Philos. T. Roy Soc. A, 369, 2087–2112, doi:10.1098/rsta.2010.0240, 2011.

Atmos. Meas. Tech. Discuss., doi:10.5194/amt-2016-127, 2016
Manuscript under review for journal Atmos. Meas. Tech.
Published: 25 April 2016
© Author(s) 2016. CC-BY 3.0 License.



Atmospheric Measurement Techniques Discussions

Tables

Table 1. Specifications of the blackbody calibration source.

Type	MIKRON M330-EU
Manufacturer	Lumasense Technologies
Temperature range	573.15 K to 1973.15 K
Temperature uncertainty	$\pm 0.025 \cdot (T - 273.15\,\mathrm{K}) \pm 1\,\mathrm{K}$
Source homogeneity	± 1 K within inner 1/3 of aperture
Aperture diameter	25 mm
Emissivity	0.99 ± 0.005

Atmos. Meas. Tech. Discuss., doi:10.5194/amt-2016-127, 2016
Manuscript under review for journal Atmos. Meas. Tech.
Published: 25 April 2016
© Author(s) 2016. CC-BY 3.0 License.



Atmospheric Measurement Techniques Discussions

Figures

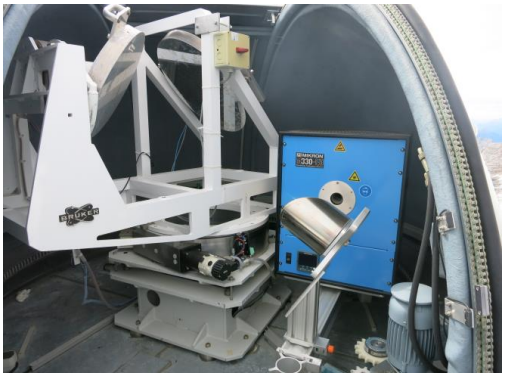


Figure 1. Blackbody calibration source inside the Zugspitze solar FTIR dome, additional 90° off-axis mirror and solar tracker.

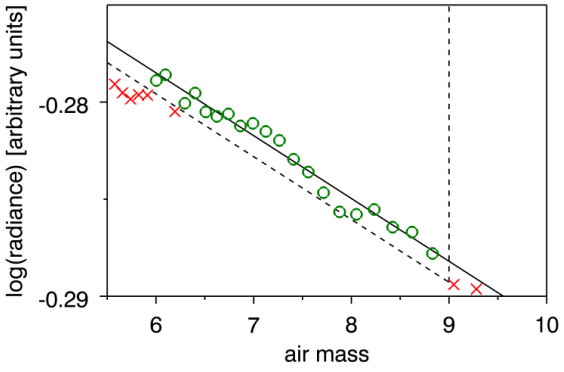


Figure 2. Selection of spectra for the Langley measurements made on 13 December 2013. Continuous black line: first estimate linear fit, dashed black line: selection threshold, green circles: selected spectra, red crosses: excluded spectra

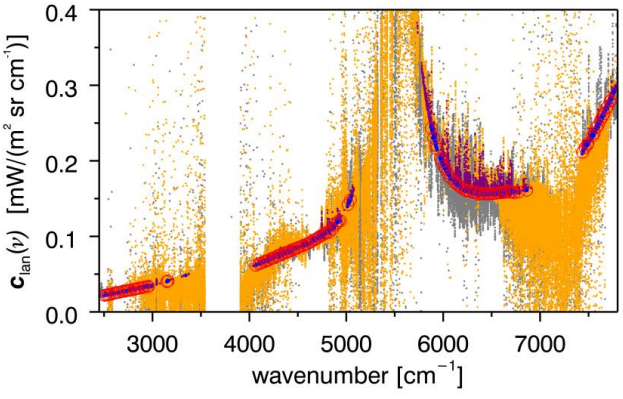


Figure 3: Selection of suitable spectral points and averaging for Langley calibration (measurements from 13 Dec. 2013). Grey: initial Langley fit results; orange: results not affected by solar lines; purple: results after applying fit uncertainty threshold; blue: final results after applying stability threshold; red circles: Langley calibration results averaged over 20 cm^{-1} bins.

Atmos. Meas. Tech. Discuss., doi:10.5194/amt-2016-127, 2016
Manuscript under review for journal Atmos. Meas. Tech.
Published: 25 April 2016
© Author(s) 2016. CC-BY 3.0 License.



Atmospheric Measurement Techniques Discussions

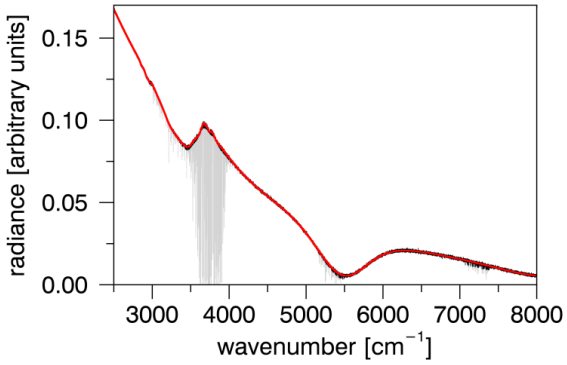


Figure 4. Blackbody radiance spectrum recorded on 24 February 2014 with a cavity temperature of 1923.15 K. Grey: measured spectrum, black: result of spectral line exclusion, red: final spectrum after median filtering.

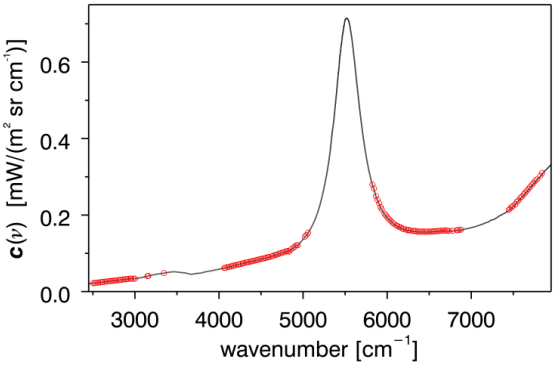


Figure 5. Combined calibration curve (black line) and selected Langley calibration points (red circles) for the Langley measurements made on 13 Dec. 2013 in combination with blackbody measurements made on 24 Feb. 2014.

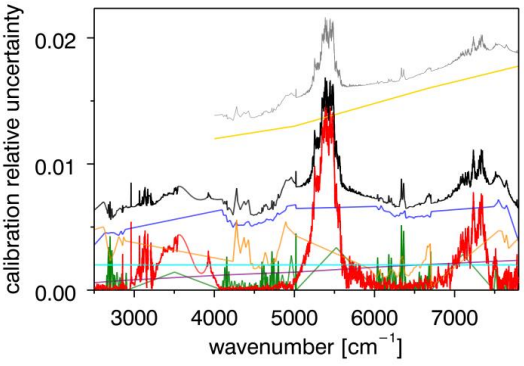


Figure 6. Relative 2-σ calibration uncertainty (Langley measurements made on 13 Dec. 2013, blackbody measurements on 24 Feb. 2014). Blue: Langley fit uncertainty, red: blackbody uncertainty, green: shape error uncertainty, orange: airmass uncertainty, purple: mispointing uncertainty, cyan: FOV uncertainty, yellow: ESS uncertainty, grey: total uncertainty, black: total uncertainty relevant for radiative closure experiment (not including ESS contribution).

Atmos. Meas. Tech. Discuss., doi:10.5194/amt-2016-127, 2016
Manuscript under review for journal Atmos. Meas. Tech.
Published: 25 April 2016
© Author(s) 2016. CC-BY 3.0 License.

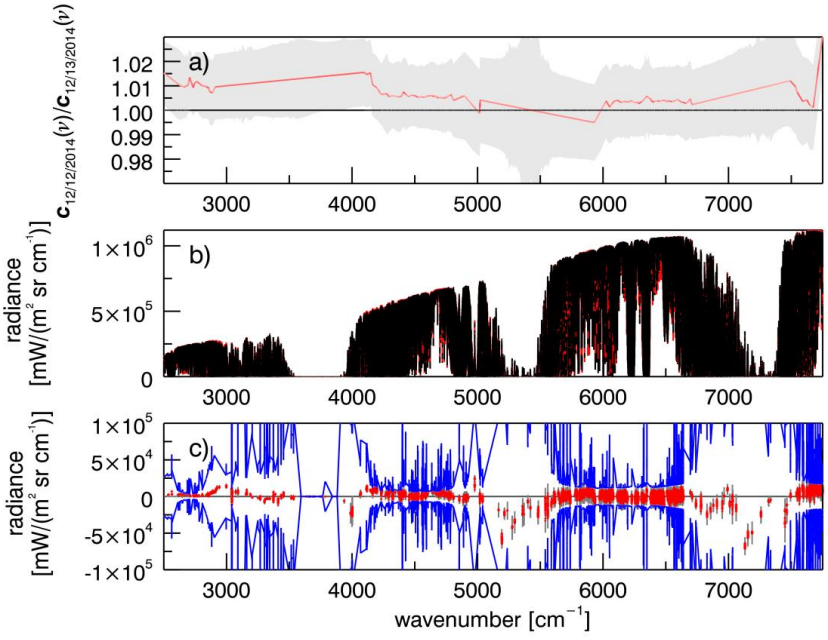


Figure 7. Validation of calibration results. a) Ratio of 12 Dec. 2013 and 13 Dec. 2013 results (red line) and 2-σ uncertainty estimate (grey shaded area). b) Mean measured (black) and synthetic (red) radiance for the validation dataset. c) Mean residual (red dots) and standard deviation of residuals (grey shaded area) for the validation dataset outside spectral lines in comparison with the 2-σ residual uncertainty estimate (blue line).